Publ. Astron. Soc. Japan **42**, 745–756 (1990)

CO ($J = 2 - 1$) Observations of the Edge-on Galaxy NGC 4631

Yoshiaki SOFUE and Toshihiro HANDA

Institute of Astronomy, University of Tokyo, Mitaka, Tokyo 181

and

Götz GOLLA and Richard WIELEBINSKI

Max-Planck-Institut für Radioastronomie, Auf dem Hügel 69, D-5300 Bonn 1, FRG

(Received 1990 June 1; accepted 1990 August 10)

Abstract

The interacting edge-on galaxy NGC 4631 has been observed in the ^{12}CO ($J = 2 - 1$) line emission using the IRAM 30-m telescope with a resolution of 13″ (330 pc). The molecular gas is strongly concentrated in a ring-like disk of 1 kpc radius. A position-velocity diagram shows that the disk is rotating almost rigidly. Individual line profiles show several velocity components, which are attributable to spiral arms within the gas disk. A comparison of the ^{12}CO ($J = 2 - 1$) and ^{12}CO ($J = 1 - 0$) data gives a line-ratio distribution along the major axis. The 2–1 to 1–0 transition line ratio is about unity on the average, indicating that the gas is opaque against the lines. However, we found some regions where the ratio significantly exceeds unity and the gas is more heated and disturbed.

Key words: CO emission; Edge-on galaxies; Gas ring; Molecular hydrogen; Tidal interaction.

1. Introduction

NGC 4631 (Arp 281) is a late-type galaxy seen nearly edge-on. It was classified as an Sc-type galaxy (Sandage 1961) or an SBd galaxy (de Vaucouleurs et al. 1976). The galaxy appears distorted, which may be due to an interaction with small companions, NGC 4627 and NGC 4656. Sandage and Tammann (1974) give the distance to this galaxy as being 5.2 Mpc, corresponding to a scale of 1 kpc/40″. An optical photograph (e.g., de Bruyn 1977) shows a patchy dust lane along the major axis, suggesting that the galaxy is rich in molecular gas. The galaxy is bright in far-infrared emission, as observed by IRAS (Lonsdale et al. 1985), while no evidence for starbursts has been reported.

H I observations (Weliachew et al. 1978) have revealed the presence of several filamentary features extending for tens of kiloparsecs from the galactic center, one of which comprises a bridge connecting NGC 4631 and NGC 4656. This H I bridge and the distorted optical morphology of NGC 4631 suggest a strong tidal interaction which has been well reproduced by a numerical simulation (Combes 1978).

Radio continuum observations (Klein et al. 1984) have indicated a bright disk component near the center, which has been resolved into several complexes (de Bruyn 1977). The galaxy has a nonthermal radio halo of a few kpc thickness, which suggests the existence of a galactic wind from the disk (Werner 1985; Lerche and Schlickerser 1981). An ordered large-scale vertical magnetic field has been detected in the halo (Hummel et al. 1988).

Evidence for a nuclear molecular gas disk has been obtained by observing the ^{12}CO ($J = 1-0$) line emission using the Nobeyama 45-m telescope (Sofue et al. 1989). It was found that the central molecular disk comprises of two ring-like structures: one at a radius of 250 pc and the other at 1 kpc, with the latter being the major part of the molecular disk. A position-velocity diagram along the major axis indicates rigid rotation. It was also shown that the tangential direction of the rings coincide with the radio continuum peaks, suggesting a tight correlation between the nonthermal radio emission and the molecular gas.

Since the CO observations were made at one transition of ^{12}CO ($J = 1 - 0$) , there has been no information about such physical conditions as the optical depth and temperature. For this we need data concerning another transition lines, and we have conducted ^{12}CO ($J = 2 - 1$) line observations of this galaxy using the IRAM 30-m telescope. Obviously, we also aim at better angular resolution ($13''$) compared with the previous 45-m observations ($17''$). In this paper we report results from the new ^{12}CO ($J = 2 - 1$) observations, and discuss physical conditions in comparison with the ^{12}CO ($J = 1 - 0$) data.

2. Observations

Observations of the ^{12}CO ($J = 2 - 1$) line of NGC 4631 were made on January 19–21, 1990, using the 30-m telescope of IRAM. The antenna had a HPBW of $13''$ at 230 GHz, corresponding to a linear scale of 330 pc. The pointing accuracy was better than $\pm 3''$ through the observations. The main-beam efficiency was $\eta_{\rm mb} = 45\%$. We used an SIS double-sideband receiver combined with a backend consisting of 512-channels $\times$ 1-MHz filter-bank spectrometer, which covered 670 km s^{-1}. The velocity resolution was 1.3 km s^{-1}. The system noise temperature was about 900–1100 K through the observations. The ^{12}CO ($J = 1 - 0$) line at 115 GHz was observed simultaneously, for which the telescope had $21''$ HPBW and $\eta_{\rm mb} = 60\%$. We used an SIS receiver combined with the same type of spectrometer as mentioned above, giving a velocity coverage of 1300 km s^{-1}, a velocity separation of 0.65 km s^{-1}, and a velocity resolution of 2.6 km s^{-1}. The system temperature at 115 GHz was about 1000–1200 K.

The used intensity scale was the main-beam temperature, $T_{\rm mb}$ ($\equiv T_{\rm A}^{*}/\eta_{\rm mb}$), corrected for the atmospheric and ohmic losses and for the mainbeam efficiency. We used both a position-switching mode and wobbling beam-switching mode by chopping the

Table 1. Adopted parameters for NGC 4631.

Type[1,2]	Sc/SBd
Inclination	Edge-on
Position angle of major axis	86°
Distance[3]	5.2 Mpc
Center position[4] ($X = 0''$, $Y = 0''$)	$\alpha_{1950} = 12^{h}39^{m}41^{s}.0$
	$\delta_{1950} = 32°48'58''$
Systemic LSR velocity[4,5]	617 km s^{-1}
Galacto-centric velocity	640 km s^{-1}

(1) Sandage (1961); (2) de Vaucouleurs et al. (1976); (3) Sandage and Tammann (1974); (4) Weliachew et al. (1978); (5) Sofue et al. (1989).

secondary mirror. The radio source 3C 273 was used both for pointing and focusing checks, and a pointing calibration was made every 1 h using radio sources 1308+326 and 1156+295. The pointing accuracy was better than $\pm 3''$ throughout the observations. The axial offset between the 115 and 230 GHz observations was less than $2''$.

The reference center position and systemic LSR velocity were adopted from Sofue et al. (1989), and are summarized in table 1 with other parameters of NGC 4631. The major axis of the galaxy is taken at PA=86°, which is approximately in the direction of E and W. In the following we take a coordinate system (X, Y) with its origin at the center position, as given above. The Xcoordinate is taken along the major axis, and Yperpendicular to it ($X > 0$ toward E and $Y > 0$ toward N).

We observed 19 points along the major axis at $-54'' < X < +54''$ (within ± 1.4 kpc from center) with a grid spacing of $6''$. We also made scans perpendicular to the major axis at $X = 0''$, $\pm 42''$ for $-24'' \leq Y \leq +24''$ with the same grid spacing. A few more points were added at $Y = \pm 12''$. In total, we observed 41 points, and spent about 20 hours. On-source integration time per each point was about 10 min, and for several points 20 min. The rms noise was $\Delta T_{\rm mb} \simeq 85$ and 85 mK for ^{12}CO ($J = 1 - 0$) and ^{12}CO ($J = 2 - 1$) data, respectively.

3. Results

(a) Spectra

Figure 1 shows the obtained ^{12}CO ($J = 2 - 1$) and ^{12}CO ($J = 1 - 0$) line spectra. The CO line has been well detected at almost all points. Figure 2 shows detailed spectra taken along the major axis. Figure 3 shows an enlargement of the spectra for the center and for $(X, Y) = (48'', 3'')$.

The ^{12}CO ($J = 2 - 1$) line profile at the center is symmetric with respect to the systemic velocity. From an eye estimate we can see that the profile apears to have two components: narrow and broad. The narrow component has a width of about 40 km s^{-1}centered at the systemic velocity, 620 km s^{-1}, while the wide component

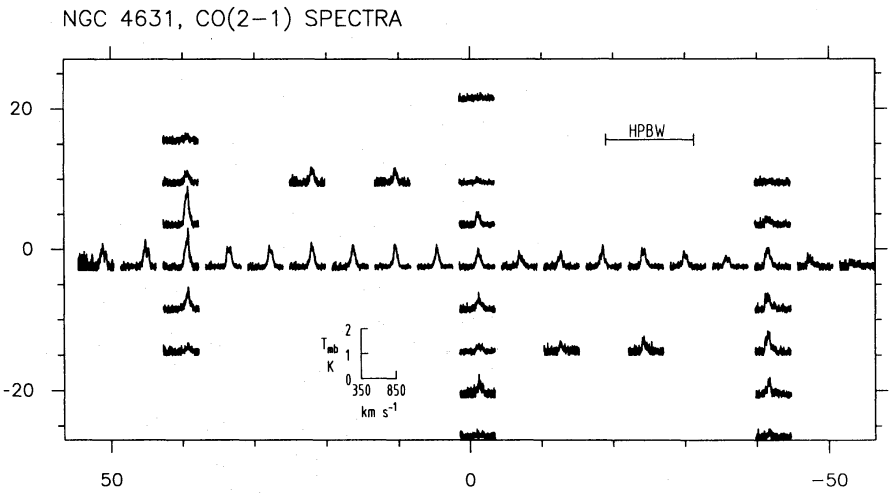

Fig. 1a. Spectra of the ^{12}CO ($J = 2-1$) line emission observed for the edge-on galaxy NGC 4631 using the IRAM 30-m telescope.

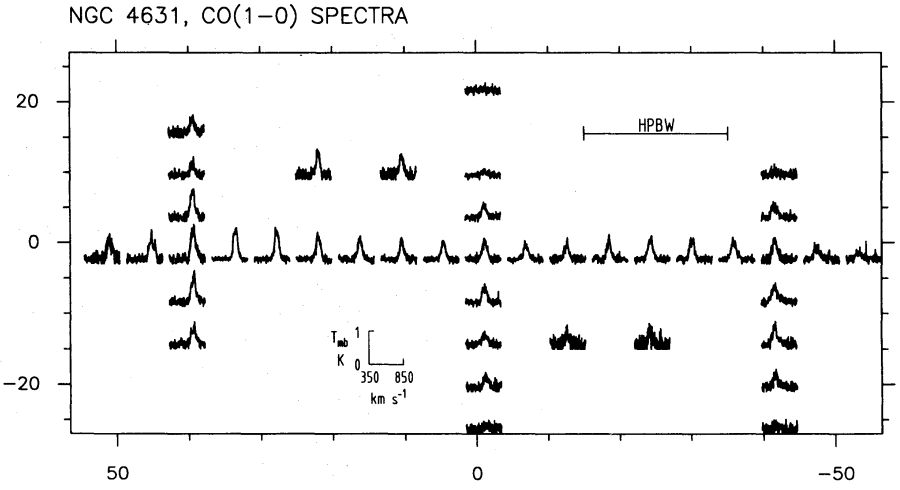

Fig. 1b. Same as in figure 1a, but for the ^{12}CO ($J = 1-0$) line emission.

nearly Gaussian with a velocity width of about 100 km s^{-1}. The narrow component corresponds to gases in the disk apart from the nucleus, the motion of which is nearly transverse to the line of sight. The broad component may be due to circum-nuclear gas clouds, which represents rotation within the beam as well as a large velocity dispersion in the nuclear disk. The highest temperature of $T_{\rm mb} \simeq 1.6$ K was observed at $X \simeq 42''$ (1 kpc). There are a few more peaks at $X = +10 - 20''$, $-18''$, and $-42''$ (see also figure 5).

Each of the profiles along the galactic plane comprises of several distinguished velocity components, an example of which can be seen for the profile shown in figure 3 for $X = 48''$. Individual velocity components may correspond to structures within

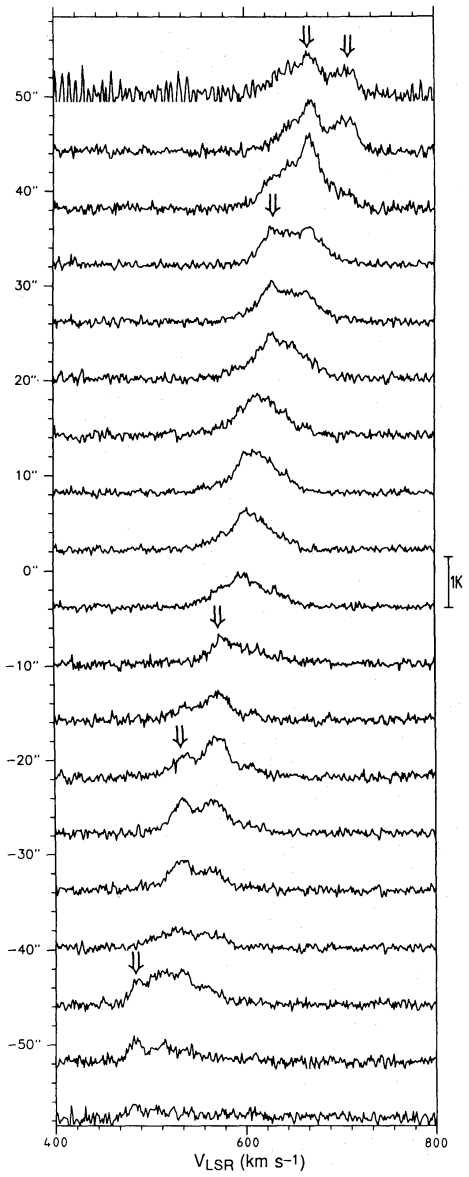

Fig. 2. ^{12}CO ($J = 2 - 1$) spectra along the major axis. The arrows indicate the major velocity componenets, which are likely attributed to spiral arms.

the galactic plane, most probably due to spiral arms. The relative intensities of the components vary from position to position, and at $X > 0''$ larger-velocity (red-shifted) components appear to become dominant as the distance from the center increases, and vice versa at $X < 0''$. The global red and blue shifts along the major axis represent galactic rotation.

(b) Position-Velocity Diagrams

Position-velocity diagrams along the major axis are shown in figure 4, where the

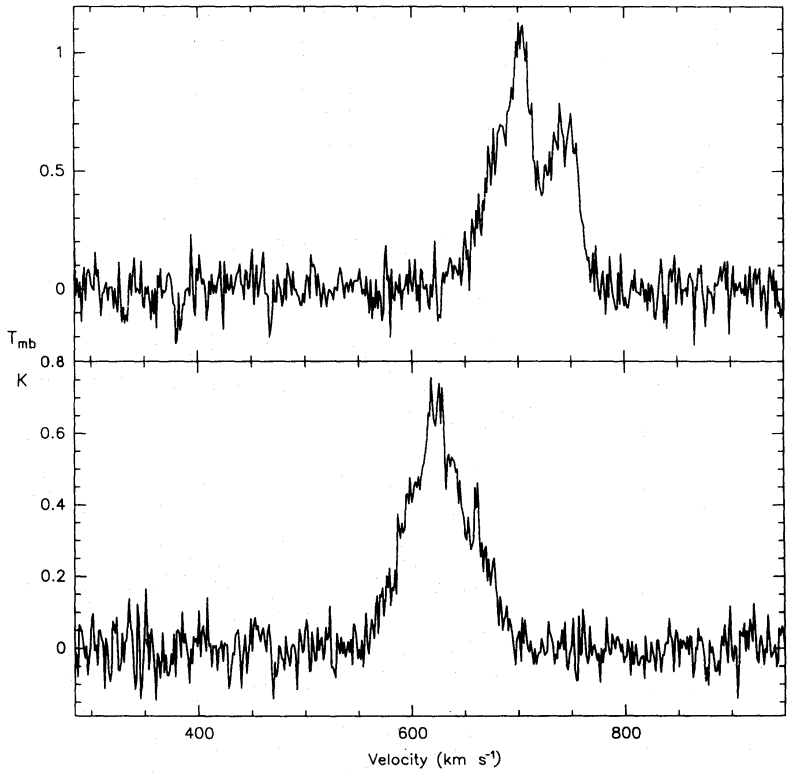

Fig. 3. ^{12}CO ($J = 2-1$) spectra taken at $(X, Y) = (0'', 0'')$ and at $(48'', 3'')$.

distibution of $T_{\rm mb}$ is shown on the X- $V_{\rm LSR}$ plane in the form of a contour diagram. The diagrams indicate a clear rotation of the central molecular disk. For an edge-on galaxy the rotation characteristics may be derived without any uncertainty regarding the inclination.

As can be seen in the diagram, the rotation velocity, V, increases almost linearly with the radius, R, and obeys a relation as given by Sofue et al. (1989):

$$V(R)\ [\mathrm{km\ s^{-1}}] \simeq 80R\ [\mathrm{kpc}]. \quad (1)$$

This may represent the inner rotation characteristics within a few kpc of the center. On the other hand the outer rotation can be seen by H I gas: H I observations (Weliachew et al. 1978) show that the velocity further increases up to $V \simeq 150$ km s^{-1}at $R \sim 2$ kpc, reaching a flat rotation at 150 km s^{-1}.

(c) Intensity Distribution

The ^{12}CO ($J = 2-1$) and ^{12}CO ($J = 1-0$) peak temperatuers and ^{12}CO ($J = 2-1$) intensity I ($= \int T_{\rm mb} dv$) are plotted in figure 5 as a function of the distance from the center. The distributions have two clear peaks at $X = \sim \pm 42''$, which appear to be nearly symmetric with respect to the center. We also find less-clear inner peaks at around $X \sim \pm 14 - 30''$. As has been suggested by Sofue et al. (1989) from their ^{12}CO ($J = 1-0$) observations, we may consider that the peaks at $X = \pm 42''$ make a

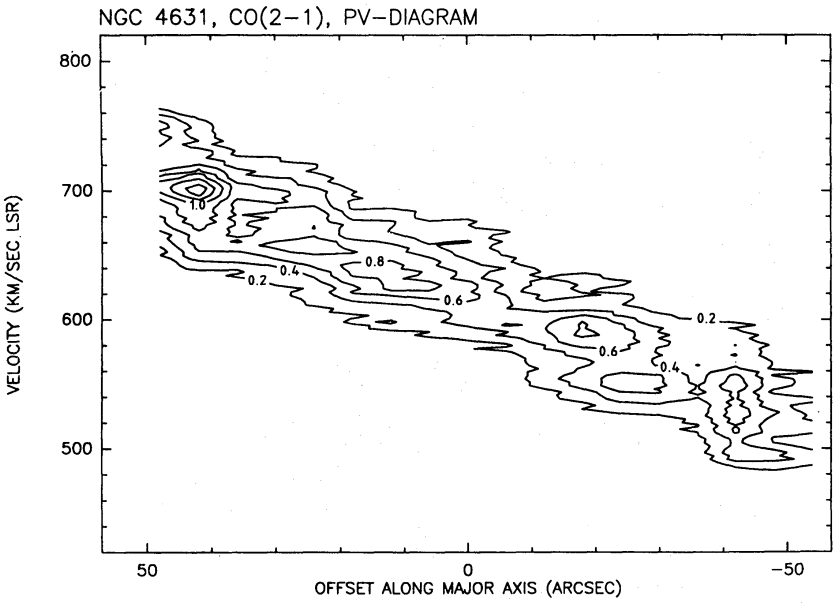

Fig. 4a. Position-velocity (X - $V_{\rm LSR}$) diagram of the ^{12}CO ($J = 2 - 1$) line emission obtained along the major axis of NGC 4631. The contours are at 0.2, 0.4, ... K $T_{\rm mb}$.

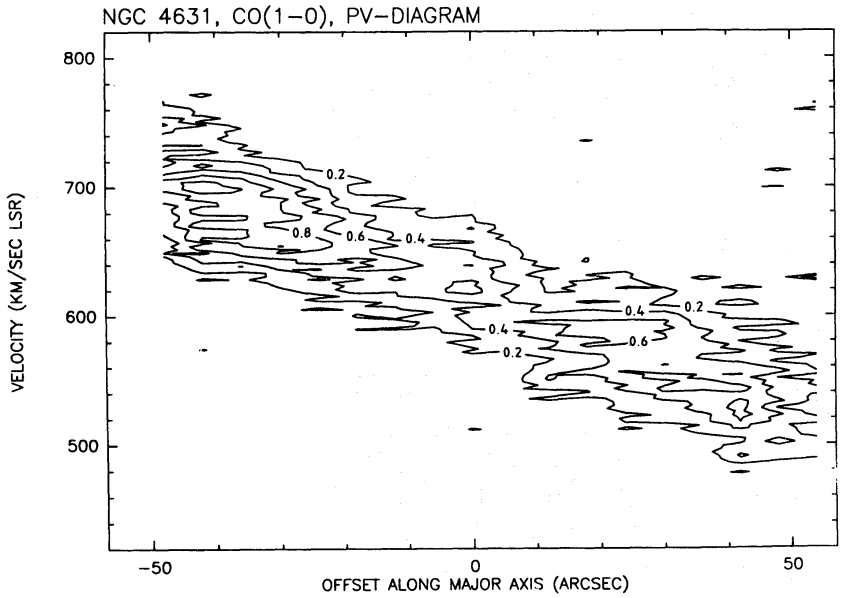

Fig. 4b. The same as in figure 4a, but for ^{12}CO ($J = 1 - 0$) line emission. Contour unit is also the same.

pair of peaks at symmetric positions with respect to the center. It seems that we also have a pair of inner, but less clear, peaks at $X = \pm 10 - 20''$. There is significant asymmetry between the eastern and western intensities: the western peak is less pronounced. The present ^{12}CO ($J = 1 - 0$) line distribution is similar to that

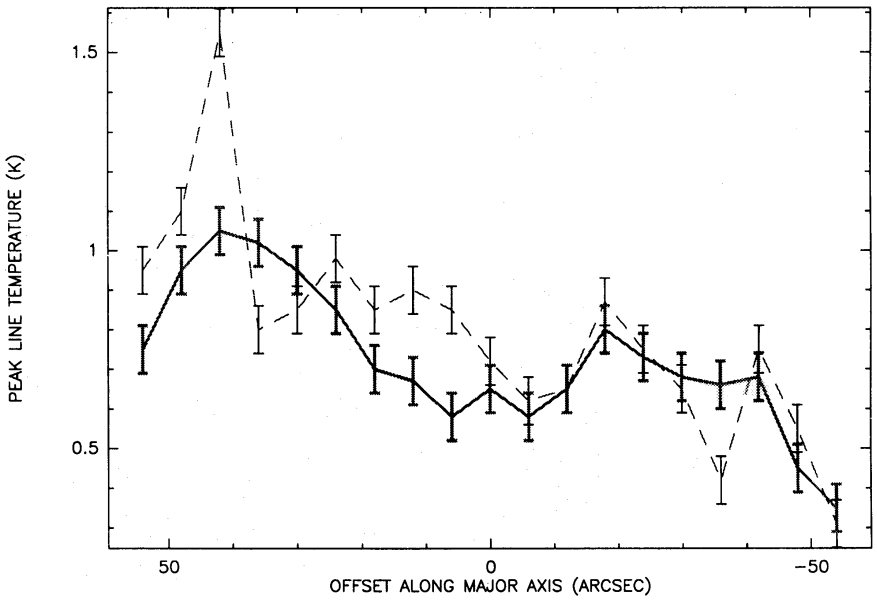

Fig. 5. Distributions of peak $T_{\rm mb}$ of the ^{12}CO ($J=2-1$) and ^{12}CO ($J=1-0$) line emissions (circles and triangles, respectively). The errors are typically $\pm$80 mK.

observed in the same line by Sofue et al. (1989), while the asymmetry is more prominent. The sharp ^{12}CO ($J=2-1$) peak at $X=+42''$ has not been detected in the lower resolution ^{12}CO ($J=1-0$) data, and we may have detected some compact, high-temperature complex toward this $+42''$ peak.

The outer two peaks at $X\sim\pm40''$ coincide with the tangential directions of the 1-kpc ring as derived by our previous ^{12}CO ($J=1-0$) 45-m observations (Sofue et al. 1989). The inner peaks also appear to be coincident with the inner 250-pc ring, although the coincidence is less clear.

We now comment on the relation of the ^{12}CO ($J=1-0$) intensity scales between the IRAM 30-m telescope and the NRO 45-m telescope. With the 45-m telescope we obtained an antenna temperature of $T_{\rm A}^{*}\sim0.2$ K, or $T_{\rm mb}\sim0.5$ K, toward $X\sim\pm40''$. With the 30-m telescope we obtained $T_{\rm mb}\sim1$ K and 0.6 K toward $X=42''$ and $-42''$, respectively. Toward the center position, 45-m gave 0.4 K, while 30-m gave 0.6 K. Hence the ratio of $T_{\rm mb}$ by 30-m to that by 45-m is about 1.5 toward the center. The ratio is also ~1.5 toward the other regions, except toward $+40''$. At $X\sim40''$ we have a ratio as large as two. Since the antenna beam of 30-m ($21''$) is larger than that of 45-m ($17''$), the true intensity scale ratio may be still larger.

This gives us some discrepancy in mass estimates for H_2 gas: the mass estimated from the 30-m telescope gives a larger value than that from 45-m. The total mass of H_2 gas is estimated by

$$M_{\rm H_2}=\int 2m_{\rm H}N_{\rm H_2}dXdY, \tag{2}$$

where

$$N_{\rm H_2}[{\rm H_2\ cm^{-2}}]=6\times10^{20}I[\ {\rm K\ km\ s^{-1}}] \tag{3}$$

is the column density (Young and Scoville 1982) and $m_{\rm H}$ is the hydrogen mass. The molecular hydrogen mass involved within $X = \pm 54''$ (observed area) as estimated from this relation applied to the 30-m data (HPBW=21″) is about $M_{\rm H_2} \sim 6 \times 10^8 M_\odot$, while for the same area the 45-m data (HPBW=17″) give $M_{\rm H_2} \sim 2 \times 10^8 M_\odot$. The dynamical (total) mass within the same area as estimated from the rotation characteristics is $M_{\rm dyn} \sim 2 \times 10^9 M_\odot$. The 30-m result then gives a relatively large value for the H_2-to-total mass ratio of about 0.3, while a ratio of about 0.1 is obtained from the 45-m data.

The discrepancy comes mainly from a systematic difference of the intensity scales of the two telescopes. Though a thorough study of error beams at both Nobeyama and Pico Veleta is necessary to resolve the issue, at this moment we have no way to calibrate the scales with each other. We, therefore, restrict our discussion only to a comparison of the two transition lines taken from the 30-m telescope. We also mention that the mass estimated here includes an error of a factor of about two in addition to the error involved in the intensity-to-mass conversion formula.

4. Discussion

(a) ^{12}CO ($J = 2-1$) / ^{12}CO ($J = 1-0$) Line Intensity Ratio

The ratio of ^{12}CO ($J = 2-1$) to ^{12}CO ($J = 1-0$) line temperatures, $r = T_{\rm mb}(2-1)/T_{\rm mb}(1-0)$, gives information about the optical depths and temperature of the gas. As can be seen from figure 5, the ratio r is nearly equal to unity as a whole, even if we take into account the difference between the HPBW of the ^{12}CO ($J = 2-1$) and ^{12}CO ($J = 1-0$) observations. However, only toward the 42″ peak, we find a larger r value: the ratio siginificantly exceeds unity, and attains $r \simeq 1.5$.

If we assume a local thermal equilibrium (LTE) for both transitions, or if the excitation temperatures for the $J = 2-1$ and $1-0$ are the same, the ratio r is expressed by

$$r = (1 - e^{-\tau_{2-1}})/(1 - e^{-\tau_{1-0}}), \tag{4}$$

where τ_{2-1} and τ_{1-0} are the optical depths of the corresponding transitions (e.g., Loiseau et al. 1989). The ratio of the optical depths is given by

$$\tau_{2-1}/\tau_{1-0} = 2[(1 - e^{-h\nu_{2-1}/kT_{\rm ex}})/(1 - e^{-h\nu_{1-0}/kT_{\rm ex}})]e^{-h\nu_{1-0}/kT_{\rm ex}}. \tag{5}$$

In the case of $\tau_{2-1},\ \tau_{1-0} \gg 1$ (optically thick) we have $r \simeq 1$. For another extreme case of $\tau_{2-1},\ \tau_{1-0} \ll 1$ (optically thin) we have $r \simeq 4e^{-5.53/T_{\rm ex}({\rm K})}$, and for a nominal value of excitation temperature, $T_{\rm ex} \sim 20$ K, we obtain $r \simeq 3$.

Thus, a line ratio of unity on the average indicates that the gas in the disk is generally optically thick, as is usually the case for molecular clouds in normal galaxy disks. However, the gas is optically thin (or at least less opaque) toward the outer +42″ peak. The thinner optical depth may be accounted for if the gas clouds have higher temperatures, or they are more disturbed to have larger inner velocity dispersion. This is, indeed, expected if we adopt a bar-induced shock model for the accretion of gas (see section 4).

(b) Gas Ring and Accretion

The present CO observations covered the central $\pm 54''$ (± 1.4 kpc) strip along the galactic plane. The intensity distribution along the major axis (figure 5) has two major peaks at $X = \pm 30 - 40''$, which indicate that the gas is not distributed in a uniform disk, for which we should have a rather round intensity distribution peaking around the center, but in a ring-like structure. Combining the data with our previous CO observations (Sofue et al. 1989), we can see that the gas is strongly concentrated in a ring of radius about 1 kpc region. As has been suggested in Sofue et al. (1989), the distribution could be alternatively explained by a model of fissioning of the gas disk, while the two possibilities, a ring or a fissioned two clumps, cannot be distinguished by the present observations.

The high concentration of molecular gas in the 1-kpc ring may be related to a tidal disturbance through an encounter with the companion galaxies, which is indicated from the distorted morphology and H I bridges between the two galaxies (Weliachew et al. 1978; Combes 1978). As a consequence of tidal interaction, a non-axisymmetric or a bar potential appears, which causes galactic shocks in the interstellar gas and results in a transfer of angular momentum (Noguchi 1988). This results in a rapid accretion of molecular gas toward the inner region, producing a dense gas disk or a ring.

Experiencing the rapid infall caused by the bar, the accreting gas clouds will collide each other. This may result in a heating of the gas and the appearence of a disturbed situation in the disk-infalling gas interface in the outer region of the disk. This yields a higher excitaion temperature and smaller scale gas clouds; the gas tends to have smaller optical depths, as has been observed toward the $+42''$ peak.

Active star formation should follow as the consequence of gas accretion. In fact the galaxy is a strong FIR emitter (Fullmer and Lonsdale 1989). Successive supernova explosions then follow and cosmic rays are accelerated. This may result in strong radio continuum emission, as observed in the inner disk/ring region (Klein et al. 1984; de Bruyn 1977).

(c) Inclination and East-West Asymmetry of the Molecular Disk

Intensity distributions perpendicular to the major axis provide information about the inclination and thickness of the disk. The intensity distributions perpendicular to the galactic plane at $X = \pm 12''$ indicate a significant displacement of the molecular gas plane from the adopted major axis: As can be seen in figure 1, the Y distribution at $X = 42''$ has a maximum at around $Y = 3 - 5''$, while at $X = -42''$ the maximum is around $Y = -6''$. Namely, the molecular disk is tilted by about 7°at $X = \pm 42''$. Since the present data do not provide a complete map around the galactic plane, we cannot discuss the warped structure in more detail.

Figure 1 also shows that the ^{12}CO ($J = 2 - 1$) emission comes from regions significantly apart from the galactic plane. Across the nucleus ($X = 0''$) the emission is well detectable from $Y = -18''$ till $+12''$. The apparent half thickness is estimated to be about $15''$, and is slightly larger than the beam size of $13''$: We may estimate the true thickness as $\delta Y = (15^2 - 13^2)^{1/2} = 7.5''$, or about 190 pc. This value seems too large for the thickness of the very inner molecular disk, and may either be due to the inclination of the disk from the line of sight or due to gas high above the

disk plane. Since we know that the molecular disk is inclined from the major axis (as described above), it is more likely that this apparent thickness comes from disk inclination from the line of sight. If we assume a true thickness of the disk to be about 50 pc (e.g., Scoville and Sanders 1987) and radius 1–2 kpc, the apparent 190 pc thickness may be explained by an inclination of about 5°. In the same manner we derive disk thickness at $X = \pm 42''$ to be about the same, which may again be due to an inclination of the outer ring from the line of sight. Moreover, we suggest that an unexpected enhancement of ^{12}CO ($J = 2 - 1$) emission at $(X, Y) = (0'', -18'')$ (figure 1) might be due to this tilted ring.

In addtition to the asymmetry with respect to the galactic plane (tilt), we find asymmetry in the distribution of CO intensity along the major axis (figures 1, 2, and 5). This intensity asymmetry is not merely caused by the high-temperature peak at $X = 42''$, but seems to be caused by a larger-scale asymmetry in the gas distribution within the disk itself: The eastern half of the disk contains more gas than in the western half.

The tilt of the molecular disk from the optical major axis is likely due to a tidal force by the companions: As shown by a numerical simulation (Combes 1978), the outer disk ($> 3 - 5$ kpc) of NGC 4631 is strongly disturbed by the tidal encounter, and some warping takes place in the sense that the eastern-outer disk warps toward the west, directing to the main perturber NGC 4656. On the other hand the very inner region, where the molecular gas disk is found, is relatively calm against a tidal disturbance. This may have caused a relative tilt of the gas disk in the central region from the outermost disk. Namely, the "true" position angle of the galactic disk, which is determined from the innermost region of the galaxy, is about 82° instead of 86°. Also, the innermost disk is not perfectly edge-on, but the inclination angle of the rotation axis is aobut 85°.

In addition to the warping, the tidal force may have also induced a large-scale shift of the distribution center of gas within the disk, which may cause the observed east-west intensity asymmetry. In fact, both the distributions of molecular (present observation) and H I (Weliachew et al. 1978) gases are shifted toward the east, or in the direction of the main perturber NGC 4656 (Combes 1978).

(d) Spiral Arms

The intensity variation along the major axis indicates that the molecular gas is distributed in two major rings. In addition to these global structures, we can recognize more structures in the line profiles. As can be seen in figures 2 and 3, individual profiles are composed of several velocity components. Naturally, the velocity components should correspond either to spiral arms (or thinner rings) or to clumps. Since each of the velocity components involves a considerable portion of the total emission (mass) of gas, they are more likely arms (rings) than clumps (clouds), and we call them arms. However, since the galaxy is edge-on and the system shows rigid rotation, we cannnot distinguish gases along the line of sight, and it is difficult to distinguish arms from rings.

As indicated in figure 2, we may trace at least three major arms (equi-velocity components on the profiles) on each of the eastern and western half of the galaxy. It seems that the three arms on either sides are located approximately symmetric with

respect to the galactic center. In addition to these major arms, we can recognize a greater number of smaller components (e.g., figure 3), which may either be attributed to bifurcated arms or to gas clouds.

This work was financially supported in part by the Japan Society of Promotion of Sciences, and by the Ministry of Education, Science and Culture under Grant No. 01420001 and 01302009 (Y. Sofue).

References

Combes, F. 1978, *Astron. Astrophys.* , **65**, 47.
de Bruyn, A. G. 1977, *Astron. Astrophys.* , **58**, 221.
de Vaucouleurs, G., de Vaucouleurs, A., and Corwin, H. G., Jr. 1976, in *Second Reference Catalogue of Bright Galaxies* (University of Texas Press, Austin), p. 174.
Fullmer, L., and Lonsdale, C. J. 1989, *Catalogued Galaxies and Quasars Observed by IRAS Survey, Version 2* (Jet Propulsion Laboratory, US Government Printing Office, Washington, D.C.).
Hummel, E., Lesch, H., Wielebinski, R., and Schlickeiser, R. 1988, *Astron. Astrophys.* , **197**, L29.
Klein, U., Wielebinski, R., and Beck, R. 1984, *Astron. Astrophys.* , **133**, 19.
Lerche, I., and Schlickeiser, R. 1981, *Astrophys. Letters*, **22**, 31.
Loiseau, N., Nakai, N., Sofue, Y., Wielebinski, R., H.-P. Reuter, and Klein, U. 1989, *Astron. Astrophys.* , in press.
Lonsdale, C. J., Helou, G., Good, J. C., and Rice, W. L. 1985, *Catalogued Galaxies and Quasars Observed in the IRAS Survey* (US Government Printing Office, Washington, D.C.).
Noguchi, M. 1988, *Astron. Astrophys.* , **203**, 259.
Sandage, A. 1961, in *The Hubble Atlas of Galaxies* (Carnegie Institution of Washington, Washington, D.C.), p. 25.
Sandage, A., and Tammann, G. A. 1974, *Astrophys. J.* , **194**, 559.
Scoville, N. Z., and Sanders, D. B. 1987, in *Interstellar Processes*, ed. D. J. Hollenbach and H. A. Thronson (D. Reidel Publishing Company, Dordrecht), p. 21.
Sofue, Y., Handa, T., and Nakai, N. 1989, *Publ. Astron. Soc. Japan*, **41**, 937.
Weliachew, L., Sancisi, R., and Guélin, M. 1978, *Astron. Astrophys.* , **65**, 37.
Werner, W. 1985, *Astron. Astrophys.* , **144**, 502.
Young, J. S., and Scoville, N. 1982, *Astrophys. J.* , **258**, 467.